Practical Aspects of Optimal Mismatch Filtering and Adaptive Pulse Compression for FM Waveforms

Dakota Henke[1], Patrick McCormick[1], Shannon D. Blunt[1], and Thomas Higgins[2]

[1]Radar Systems Lab, University of Kansas, Lawrence, KS
[2]Radar Division, US Naval Research Laboratory, Washington, DC

***Abstract*—The sensitivity impact of range straddling in the form of mismatch loss is well known. What is less appreciated, however, is the effect upon dynamic range, particularly for receive filtering that seeks to minimize range sidelobes. For FM-based waveforms, which are readily implementable in a high-power radar system, it is shown that least-squares (LS) mismatched filtering (MMF) realizes a penalty in sidelobe suppression when range straddling occurs. This degradation can be partially compensated through modification of the LS MMF implementation. Alternatively, adaptive pulse compression (APC), appropriately modified for application to FM waveforms, demonstrates robustness to both straddling and eclipsing effects. Simulated and experimentally measured results are provided to demonstrate the efficacy of these filtering approaches.**

I. INTRODUCTION

For a given radar waveform, the "goodness" of the associated pulse compression receive filter is determined by metrics such as peak sidelobe level (PSL), integrated sidelobe level (ISL), and mismatch loss. Mismatch loss is generally defined as the mainlobe peak of a mismatched filter (MMF) relative to the mainlobe peak of the matched filter for the same noise power output from each. The MMF presumably provides greater sidelobe suppression as the trade-off for mismatch loss.

Range straddling arises when the received, sampled replica of the transmitted radar waveform does not perfectly coincide with the sampled version of the waveform used to construct the receive filter [1]. It is well known that this form of mismatch loss, which even occurs for the matched filter, is reduced by increasing the sampling rate for both the received signal and the filter (see, for example, [2]). Alternatively [3] addresses the problem of range straddling by incorporating all analog and digital system filters into a composite analog response for subsequent design of a compensating filter.

For polyphase codes (see Chap. 6 of [4]), notwithstanding the difficulty in generating them as physical waveforms with high fidelity, the chip transitions represent a source of potentially significant mismatch loss due to straddling. However, for FM-based waveforms, which are far more commonly used with high-power systems, their inherently continuous nature translates into a rather small loss from straddling with only modest "over-sampling" required (relative to the 3 dB bandwidth) [2]. For these reasons we limit our consideration to FM waveforms (also noting that polyphase codes can be implemented as FM waveforms via [2] and optimized as such [5]).

Optimized mismatched filtering, where the filter is typically obtained via Least Squares (LS) [6] or possibly via L_p norm minimization [7,8], can achieve sidelobe levels much lower than the matched filter (depending on the waveform) while incurring a rather small mismatch loss. Being non-adaptive, the LS MMF seeks to minimize the sidelobe response at all delay shifts included in the signal model as it is unknown a priori which, if any, relative delays require lower sidelobes (since the range profile is unknown). Oversampling (with respect to waveform 3 dB bandwidth) can also be performed for the LS MMF [2] by employing "beam spoiling" to prevent an increase in sidelobes that arise in conjunction with range super-resolution [9] and by diagonal loading to set the acceptable level of mismatch loss [2]. However, as shown in the subsequent section, the achievable sidelobe performance of the LS MMF is also affected by straddling which acts as a model mismatch effect. As a result, the theoretical and practical sidelobe level performance realized by LS MMF can differ by orders of magnitude for some FM waveforms.

It is possible to at least partially compensate for this model mismatch effect without the need for further oversampling through a straightforward modification to the LS filter implementation. However, to regain nearly all of the sensitivity lost by LS MMF under the straddling condition necessitates receive adaptivity in the range domain. The adaptive pulse compression (APC) algorithm [10] has been shown to provide this capability for polyphase codes and here, following small modifications to account for the structural difference and the need for oversampling, is demonstrated to do so for FM waveforms as well.

II. LS MISMATCHED FILTERING OF FM WAVEFORMS

Let the transmitted radar waveform be denoted as $s(t)$ with pulsewidth T. Define the receive sampling period as

$$T_S = \frac{T}{K(BT)} = \frac{T}{N}, \tag{1}$$

where BT is the waveform time-bandwidth product. The pulse rise-time and fall-time are assumed negligible and bandwidth implies the 3 dB bandwidth, where K indicates the degree of "over-sampling" relative to 3 dB bandwidth (with $3 < K < 5$ found to work well for the filtering schemes considered here). The value $N = K(BT)$ is therefore the number of samples in a discretized representation of the waveform, which is denoted as the vector $\mathbf{s} = [s_1 \; s_2 \; \cdots \; s_N]^T$.

The LS formulation from [6] uses $\mathbf{s}$ to form the matrix of dimension $((M+1)N-1) \times MN$ as

This work was supported in part by the Radar Division of the Naval Research Laboratory and the Air Force Office of Scientific Research.

$$\mathbf{A} = \begin{bmatrix} s_1 & 0 & \cdots & 0 \\ \vdots & s_1 & & \vdots \\ s_N & \vdots & \ddots & 0 \\ 0 & s_N & & s_1 \\ \vdots & & \ddots & \vdots \\ 0 & \cdots & 0 & s_N \end{bmatrix}, \quad (2)$$

with MN the length of the LS MMF and M typically on the order of 2 to 4. Applying the traditional LS approach from [6] and modifying for FM waveforms as described in [2] yields the filter

$$\mathbf{h} = \left(\tilde{\mathbf{A}}^H \tilde{\mathbf{A}} + \delta \mathbf{I}\right)^{-1} \tilde{\mathbf{A}}^H \mathbf{e}_m, \quad (3)$$

where δ is a diagonal loading factor, $\mathbf{I}$ is a $MN \times MN$ identity matrix, $\mathbf{e}_m$ is the length $(M+1)N-1$ elementary vector with a 1 in the mth element and zero elsewhere, and $(\bullet)^H$ denotes the complex conjugate transpose. The matrix $\tilde{\mathbf{A}}$ is the same as the matrix $\mathbf{A}$ except with some number of rows above and below the mth row replaced with zeros to provide the beam-spoiling described earlier. The precise number of zeroed rows in $\tilde{\mathbf{A}}$ to achieve the nominal resolution of the matched filter is dependent on the waveform and the value of K. Here the number of rows is set such that mismatch loss is minimized.

Figure 1 illustrates the matched filter and LS MMF responses (using M = 4) for a linear frequency-modulated (LFM) waveform generated via the polyphase-coded FM (PCFM) framework in [5] with time-bandwidth product of 64. The waveform and filters are sampled at K = 5 times the 3 dB bandwidth. Both filter responses are based on the idealized scenario in which no range straddling occurs, where the matched filter achieves a PSL of –13.8 dB and the LS MMF a PSL of –66.5 dB, an improvement of nearly 53 dB. Note, however, that the MMF realizes small spurious peaks (around the –70 dB level) which could be problematic for a subsequent detection stage in a high dynamic range scenario.

Figure 2 shows the matched filter and LS MMF responses (M = 4) for the optimized (PCFM) waveform denoted as 'performance diversity' from [5] with time-bandwidth product of 64. The waveform and filters again use K = 5. Both filter responses are likewise based on the idealized scenario of no range straddling. For this optimized FM waveform the matched filter achieving a PSL of –40.2 dB and the LS MMF a PSL of –77.3 dB, an improvement of nearly 37 dB. Compared to the LFM case, the outermost spurious peaks for the MMF are now more rounded while those occurring near the edges of the matched filter response are pushed down an additional 10 dB to around the –80 dB level.

Where Fig. 2 depicts the filter responses for ideal sampling, now consider Fig. 3 in which the sampling of the received waveform (assuming reflection from a point scatterer) is offset in delay by $0.5T_S$, representing the "worst case" range straddling. Here it is observed that, while the matched filter PSL increases by less than 2 dB, the LS MMF sidelobes have increased by approximately 25 dB. Though the associated PSL value of –50.0 dB for the MMF is still 11.8 dB better than that of the matched filter, it is clear that the MMF sensitivity to range straddling is rather significant. Of course, the spurious peaks observed in Figs. 1 and 2 have now disappeared.

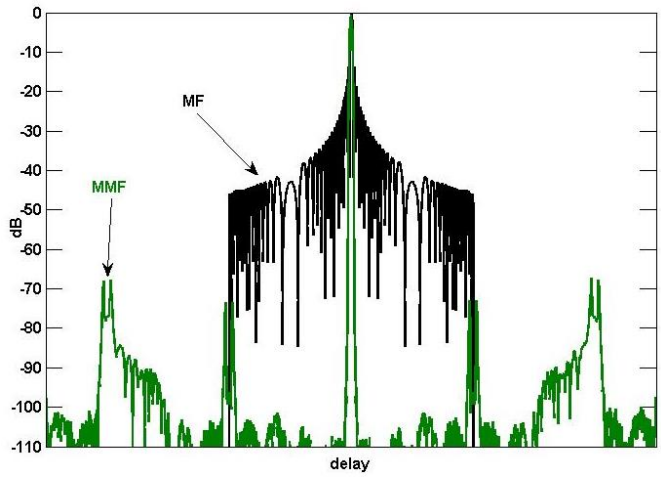

Fig. 1. MF and LS MMF (M = 4, K = 5) responses for LFM waveform

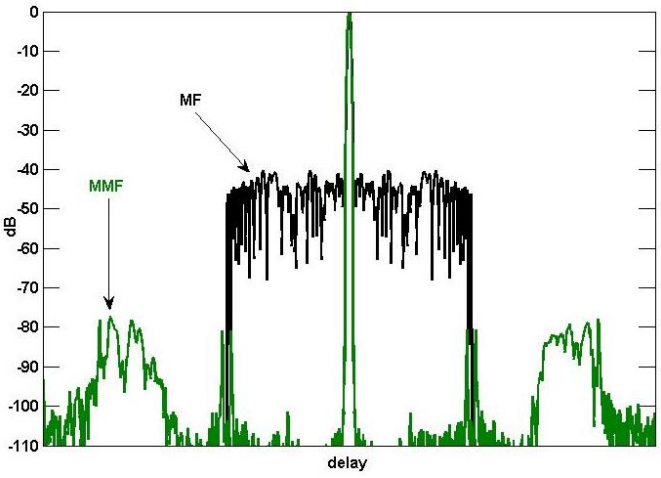

Fig. 2. MF and LS MMF (M = 4, K = 5) responses for 'performance diversity' optimized FM waveform [5]

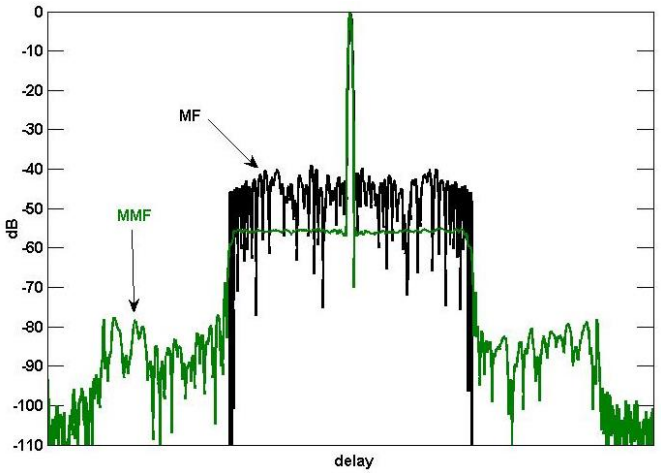

Fig. 3. MF and LS MMF (M = 4, K = 5) responses for 'performance diversity' optimized FM waveform [5] for worst-case range straddling

To provide a more comprehensive evaluation of straddling effects on the LS MMF for FM waveforms, Table I provides the PSL values of LS MMF responses for each of the five optimized FM waveforms from [5] with K = 3 or 5 for the cases of no straddling and worst-case straddling. Aside from the 'PSL-only' waveform (where the name implies the optimization metric used) the MMF responses results in more than 20 dB PSL degradation for the K = 3 sampling for worst-case straddling relative to the ideal condition. A similar trend is observed for K = 5.

TABLE I. STRADDLING EFFECTS ON PSL FOR LS MMF FOR OPTIMIZED FM WAVEFORMS FROM [5]

	PSL with no straddling (dB)		PSL with straddling (dB)	
Waveform	**K = 3**	**K = 5**	**K = 3**	**K = 5**
LFM	–67.0	–66.5	–46.3	–50.8
ISL-only	–68.4	–74.2	–46.4	–52.9
PSL-only	–41.2	–41.8	–39.8	–46.5
FTE-only	–67.9	–69.0	–42.3	–49.5
Perf. Div.	–74.8	–77.3	–49.7	–54.8

The degradation of LS MMF sidelobes due to range straddling can be partially mitigated by performing a simple averaging procedure. Segment the sampling period T_S into L equal sub-sampling delay offsets denoted by $\ell T_S/L$ for $\ell = 0, 1, 2, \cdots, L-1$. Using the original continuous version of the waveform $s(t)$, now L discretized versions can be obtained denoted as $\mathbf{s}_{N,\ell}$, where each is generated by introducing the relative delay offset of $\ell T_S/L$ to $s(t)$ prior to discretizing.

Using each of these L discretized versions of the waveform, an associated LS MMF can be formed using (2) and (3) to obtain the set of filters $\mathbf{h}_\ell$ for $\ell = 0, 1, 2, \cdots, L-1$. Clearly these filters will be nearly identical to one another since the discretized waveforms $\mathbf{s}_{N,\ell}$ are also nearly identical. However, because the goal is to achieve ever lower sidelobe levels these small differences play an important role. While we cannot drive the sidelobes to the level achieved in the idealistic straddling-free condition, up to a few additional dB of sidelobe reduction can be achieved by simply averaging over the set of filters as

$$\bar{\mathbf{h}} = \frac{1}{L}\sum_{\ell=0}^{L-1}\mathbf{h}_\ell \; . \tag{4}$$

Again using the 'performance diversity' waveform [5] as an example, Fig. 4 illustrates the MMF response using (3) which corresponds to L = 1 and the response from using (4) with L = 5. It is observed that roughly 4 dB PSL improvement is obtained using this MMF filter averaging procedure. While by no means a revolutionary improvement, this modification requires no additional implementation cost aside from the off-line design process. Likewise for the other waveforms discussed above, an improvement of 2 to 6 dB in PSL is realized.

PSL improves monotonically as L is increased, though the degree of improvement diminishes at each increase in L. This averaging also has the effect of flattening the spurious peaks observed in Figs. 1 and 2 when no straddling occurs. Overall, the averaging in (4) has the effect of compressing the difference in PSL between the best-case delay and worst-case straddling condition. For example, for the same 'performance diversity' waveform [5] using M = 4 and K = 5, the MMF from (3) realizes PSL values that vary over the delay offset interval $[0, T_S]$ by –74 < PSL < – 50 dB, a 24 dB variation. When L = 5 is used for averaging as in (4), the possible PSL values are compressed to –69 < PSL < – 54 dB (a 15 dB variation) and the spurious peaks are smeared out thus preventing their false detection as seemingly small targets. If L = 20 were used the top end (worst case) lowers 1 dB more to – 55 dB with no change to the low end PSL.

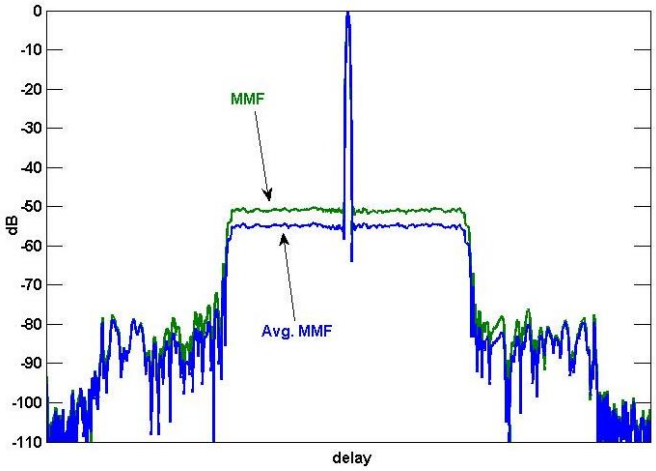

Fig. 4. LS MMF worst-case straddling responses for 'performance diversity' optimized FM waveform [5] for L = 1 and L = 5 from (4)

III. ADAPTIVE PULSE COMPRESSION OF FM WAVEFORMS

The adaptive pulse compression (APC) algorithm was developed in [10] based on an iterative implementation of minimum mean-square error (MMSE) estimation that essentially operates like a form of adaptive beamforming in the range domain. Where the matched filter and LS MMF are static, APC involves the determination of a specific filter for the estimation of each range cell (or range/Doppler cell [11,12]) in which the adaptivity of the filters is driven in a bootstrapping manner by an initial estimate of the range (or range/Doppler) profile obtained by the matched filter or MMF.

The original APC algorithm [10] was derived under the implicit assumption of using polyphase codes. Given that FM-based waveforms have much broader utility in practice as they are more amenable to high-power transmitters and provide better spectral containment, it is worthwhile to consider how APC can be applied to such waveforms. The key difference lies in the mathematical representation whereby a code is usually defined by the set of chip phase values (which is a far under-sampled representation according to Nyquist, by the way) while an FM waveform can be discretized as discussed in Section II. While the latter is still under-sampled with respect

to Nyquist (since a time-limited pulse has theoretically infinite bandwidth), the good spectral roll-off generally indicative of FM waveforms means "over-sampling" with respect to 3 dB bandwidth will maintain sufficient fidelity for APC.

Define the received signal at the radar generated by emitted waveform $s(t)$ as

$$y(t) = s(t) * x(t) + u(t), \tag{5}$$

where $x(t)$ is the illuminated range profile, $u(t)$ is additive noise, and $*$ is convolution. Like the LS formulation, a discretized version can then be represented as

$$y(n) = \mathbf{x}^T(n)\,\mathbf{s} + u(n), \tag{6}$$

for $\mathbf{s}$ the length-N sampled version of $s(t)$. Collecting N contiguous samples of (6) into the vector $\mathbf{y}(n)$, the matched filter estimate can be written as

$$\hat{x}_{\mathrm{MF}}(n) = \mathbf{s}^H\,\mathbf{y}(n)\ . \tag{7}$$

It has been found that for FM waveforms the APC algorithm is more robust to straddling effects when implemented using the decimated version of fast adaptive pulse compression (FAPC) [13], with the decimation factor equal to the waveform 3 dB over-sampling K. Further, forgoing the updating mechanism based on Woodbury's identity described in [10] avoids the resulting matrix ill-conditioning effects discussed in [10,14] as well as the need for subsequent measures to remediate them. As such, quantization effects become the limiting factor on achievable dynamic range.

Application of the MMSE formulation in [13] along with inclusion of the unity gain constraint from [15] yields the cost function

$$\begin{aligned} J(n) = \sum_{k=0}^{K-1} E\left[\left|\frac{1}{K}x(n) - \mathbf{w}_k^H(n)\,\mathbf{y}_k(n)\right|^2\right] \\ + \mathrm{Re}\left\{\lambda\left(\sum_{k=0}^{K-1}\left(\mathbf{w}_k^H(n)\,\mathbf{s}_k\right) - 1\right)\right\} \end{aligned} \tag{8}$$

for k = 1, 2, …, K, where $\mathbf{w}_k(n)$, $\mathbf{y}_k(n)$, and $\mathbf{s}_k$ are length-N/K polyphase-decomposed versions of $\mathbf{w}(n)$, $\mathbf{y}(n)$, and $\mathbf{s}$, respectively. The kth sub-filter results in the familiar MVDR-like form

$$\mathbf{w}_k(n) = \frac{\left(\mathbf{C}_k(n) + \mathbf{R}_k\right)^{-1}\mathbf{s}_k}{\sum_{i=0}^{K-1}\mathbf{s}_i^H\left(\mathbf{C}_i(n) + \mathbf{R}_i\right)^{-1}\mathbf{s}_i}, \tag{9}$$

in which $\mathbf{R}_k$ is the kth decimated $N/K \times N/K$ noise covariance matrix and $\mathbf{C}_k(n)$ is the kth decimated structured signal correlation matrix defined as

$$\mathbf{C}_k(n) = \sum_{\tau=-N+1}^{N-1} \rho(n+\tau)\ \mathbf{s}_{k,\tau}\mathbf{s}_{k,\tau}^H\ . \tag{10}$$

The term $\rho(n) = |\hat{x}(n)|^2$ in (10) is the power in the nth range cell estimated via prior matched filtering such as in (7), LS MMF, or a previous stage of APC, with

$$\mathbf{s}_{k,\tau} = \begin{Bmatrix} [s_{k-\tau} & s_{k-\tau+K} & \cdots & s_{k-\tau+K(N-1-\tilde{\tau})} & \mathbf{0}_{1\times\tilde{\tau}}]^T & \text{for} & \tau \le 0 \\ [\mathbf{0}_{1\times\tilde{\tau}} & s_{k-\tau+K\tilde{\tau}} & s_{k-\tau+K(\tilde{\tau}+1)} & \cdots & s_{k-\tau+K(N+1)}]^T & \text{for} & \tau > 0 \end{Bmatrix} \tag{11}$$

for the down-sampled delay factor

$$\tilde{\tau} = \begin{Bmatrix} \left\lfloor \dfrac{k-\tau}{K} \right\rfloor & \text{for} & \tau \le 0 \\ \left\lfloor \dfrac{K-1-(k-\tau)}{K} \right\rfloor & \text{for} & \tau > 0 \end{Bmatrix} \tag{12}$$

and $\lfloor \bullet \rfloor$ the floor operation.

As an additional modification for application to FM waveforms, the $K-1$ range indices on either side of the current range index n in (10) are, for the purpose of computing $\mathbf{w}(n)$, set to

$$\rho(n \pm k) = 0 \tag{13}$$

for k = 1, 2, … , $K-1$. This "beamspoiling" procedure has the effect of preventing the adaptive filter from forcing a range super-resolution condition [9] that can result in mismatch loss. This approach is essentially the same as that employed for the LS MMF in [2] for application to FM waveforms.

It is also necessary to address pulse eclipsing such as via the approach described in [16] or [17] to prevent a collapsing of the range window at successive adaptive stages. Denoting the non-eclipsed range cell indices as the interval $n = 0, 1, \cdots, Q-1$, the kth decimated APC filter for each of the $q = 1, 2, \cdots, N-1$ "early" eclipsed samples is

$$\mathbf{w}_k(n = -q) = \frac{\|\mathbf{s}_{N,-q}\|}{\|\mathbf{s}_N\|}\frac{\left(\mathbf{C}_k^{(n)}(0) + \mathbf{R}_k\right)^{-1}\mathbf{s}_{k,-q}}{\sum_{i=0}^{K-1}\left(\mathbf{s}_{i,-q}^H\left(\mathbf{C}_i^{(n)}(0) + \mathbf{R}_i\right)^{-1}\mathbf{s}_{i,-q}\right)} \tag{14}$$

and the kth decimated filter for each of the $q = 1, 2, \cdots, N-1$ "late" eclipsed samples is

$$\mathbf{w}_k(n = Q-1+q) = \frac{\|\mathbf{s}_{N,q}\|}{\|\mathbf{s}_N\|}\frac{\left(\mathbf{C}_k^{(n)}(Q-1) + \mathbf{R}_k\right)^{-1}\mathbf{s}_{k,q}}{\sum_{i=0}^{K-1}\left(\mathbf{s}_{i,q}^H\left(\mathbf{C}_i^{(n)}(Q-1) + \mathbf{R}_i\right)^{-1}\mathbf{s}_{i,q}\right)}\ , \tag{15}$$

where $\mathbf{s}_{k,-q}$ and $\mathbf{s}_{k,q}$ have the delay-shift structure of (11). The terms $\|\mathbf{s}_{N,-q}\|/\|\mathbf{s}_N\|$ and $\|\mathbf{s}_{N,q}\|/\|\mathbf{s}_N\|$ in (14) and (15) prevent over-compensation by the unity gain constraint. The correlation matrices $\mathbf{C}_k^{(n)}(0)$ and $\mathbf{C}_k^{(n)}(Q-1)$ are similar to the formulations when n = 0 and $n = Q-1$, the only difference being the range indices that are zeroed for "beamspoiling".

Where the LS MMF realizes an overall increase in sidelobe levels due to range straddling, this APC filter for a given range cell estimate imposes nulls at the relative delay offsets of large scatterers. Such nulls are less affected by straddling mismatch because the null width is generally sufficient to still null the interfering scatterer despite the small mismatch.

IV. Simulation Results

Since the LS MMF has been shown to improve the sensitivity of the filter response, with respect to sidelobe level, the LS MMF is here used to initialize the APC algorithm. In the following, the 'performance diversity' waveform [5] is used with $K = 5$. The APC algorithm performs two adaptive stages following the MMF initialization. Stated SNR values refer to post coherent integration.

The first two simulations consist of a large target with 80 dB SNR and a small target with SNR of 15 dB. The two targets are separated by 5 range cells (25 samples using $K = 5$). The range interval is comprised of 200 range cells (1000 samples). Figure 5 depicts the MF (black), Avg. MMF (blue), and APC (red) responses when no range straddling is present. The sidelobes are relatively low but only the Avg. MMF and APC are able to completely suppress them so that both targets are visible.

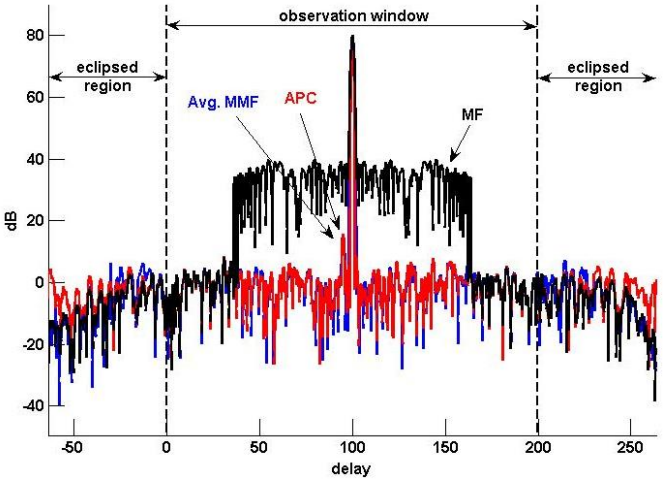

Fig. 5. LS MMF and APC responses for 'performance diversity' waveform [5] for two target scenario without straddling

Now consider the impact of range straddling. Figure 6 presents the same two-target scenario, albeit with both targets now offset in delay to realize worst-case range straddling. Similar to what was observed in Figs. 3 and 4 the Avg. MMF, while somewhat better than the original MMF, can no longer uncover the small target due to mismatch induced sidelobes. However, the APC algorithm as modified here for application to FM waveforms has no difficult discerning the small target.

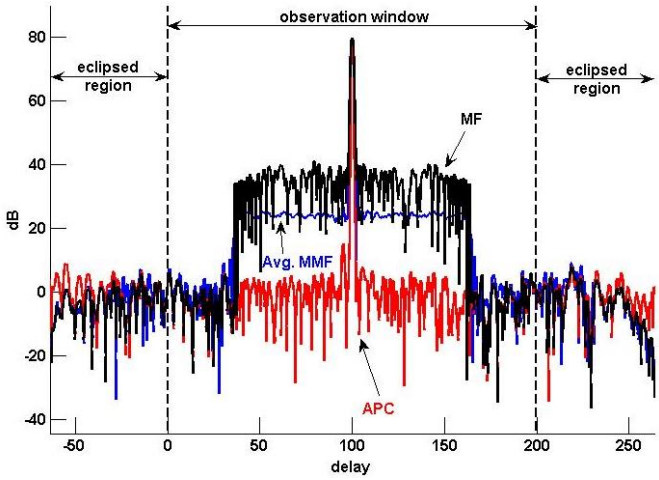

Fig. 6. LS MMF and APC responses for 'performance diversity' waveform [5] for two target scenario with straddling

Finally, consider a scenario involving numerous targets, both inside the observation window and in the pulse eclipsed regions, with disparate power levels. Here 20 targets are randomly distributed in range with SNR randomly assigned according to a uniform distribution on the interval [15, 80] dB. To demonstrate a stressing case, all received target responses are sampled at the worst-case straddling delay offset. Figure 7 shows the resulting MF, Avg. MMF, and APC responses. The MMF once again out-performs the MF, though the straddling effect clearly limits the MMF sidelobe suppression. Further, the eclipsed targets represent a different form of model mismatch for the MMF that produces additional degradation (specifically note the large eclipsed targets beyond range index 200). In contrast, APC suppresses the straddle-mismatch induced sidelobes as well as the eclipsed sidelobes. Note that APC would experience SNR loss for the eclipsed targets (relative to full power of the target echo) which is to be expected since the full power for these targets is not received since they are eclipsed.

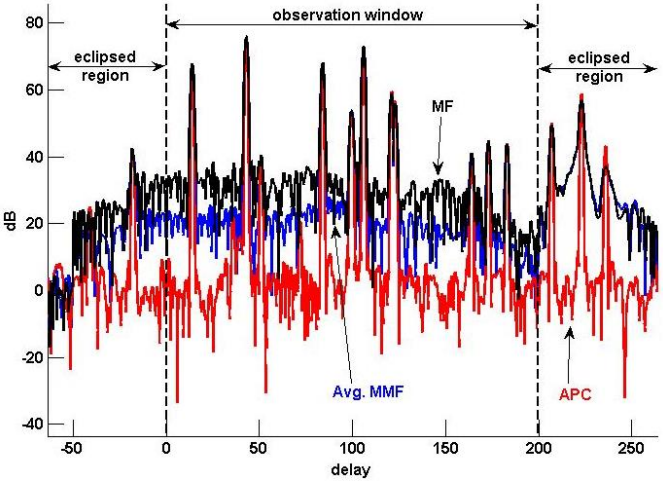

Fig. 7. LS MMF and APC responses for 'performance diversity' waveform [5] for random target scenario with straddling

V. Experimental Results

To verify the performance observed in simulation, experimental measurements were taken using the quasi-monostatic test setup shown in Fig. 8, with the field of view depicted in Fig. 9 (test setup location indicated by the star at the bottom of the figure). A standard LFM waveform was used along with the 'performance diversity' waveform from [5]. Both waveforms have a time-bandwidth product of ~64 and occupy 80 MHz bandwidth. The center frequency was 2.3 GHz and the transmit power was 24 dBm.

Fig. 8. Test setup for experimental measurements

Fig. 9. Annotated field of view for measured results

Figures 10 and 11 show the different filtering techniques applied to the LFM waveform measurements and normalized by the direct path response. The pulse compressed response resulting from the direct path provides the means to illustrate the effectiveness of the two mismatched filter (MMF) approaches and APC for sidelobe suppression. The MMF approach from (3) reveals roughly 10 dB improvement over the matched filter (MF), with about 1 dB further improvement by the averaged MMF from (4). The sidelobes preceding the direct path response are reduced by an additional 20 dB via the APC formulation above, with more modest enhancement thereafter in range.

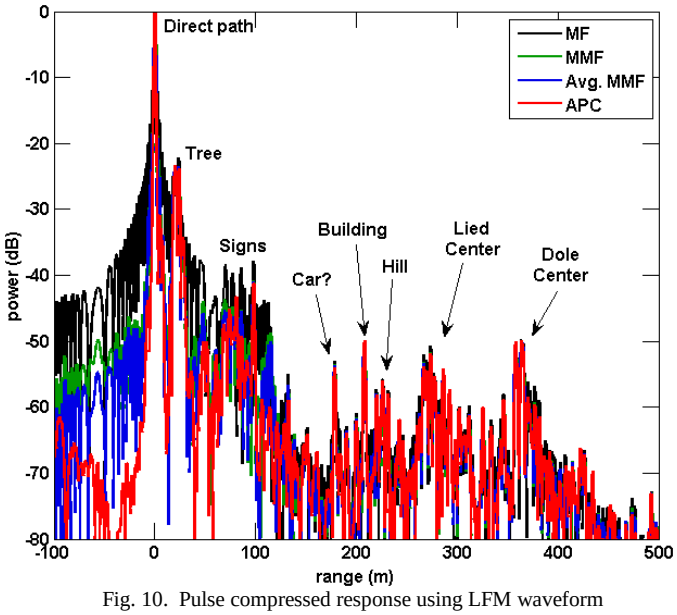

Fig. 10. Pulse compressed response using LFM waveform

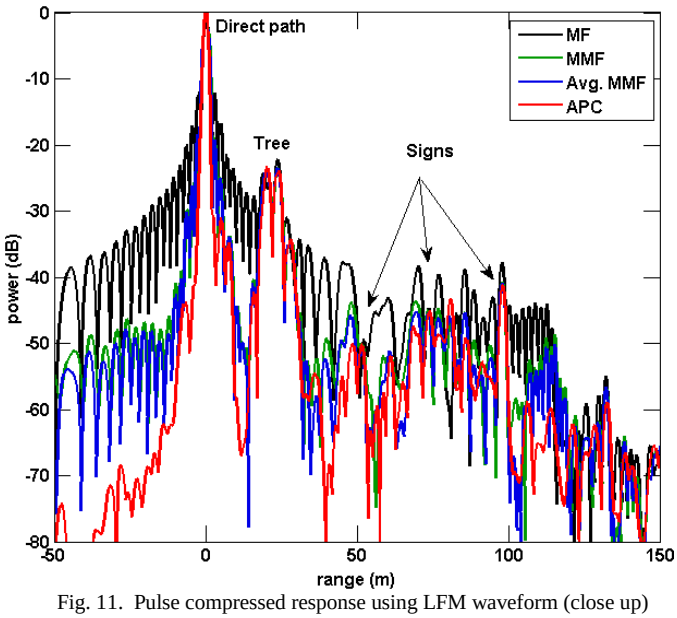

Fig. 11. Pulse compressed response using LFM waveform (close up)

Figures 12 and 13 show the different filtering techniques applied to the measurements resulting from emission of the 'performance diversity' waveform from [5] and likewise normalized by the direct path response. This optimized waveform provides much lower sidelobes to begin with for the MF and thus less overall improvement is possible. That said, examining the sidelobes preceding the direct path response, the MMF from (3) still yields about 10 dB sensitivity enhancement, with the average MMF from (4) and APC providing an additional 10 dB improvement.

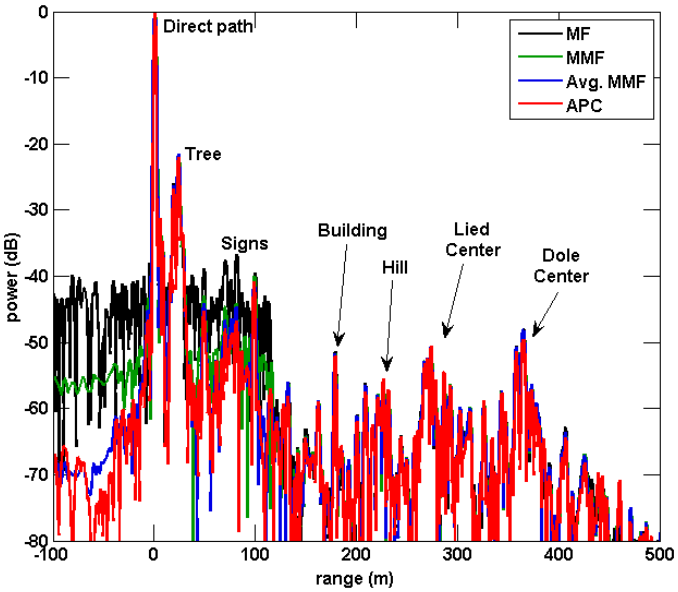

Fig. 12. Pulse compressed response using optimized FM waveform from [5]

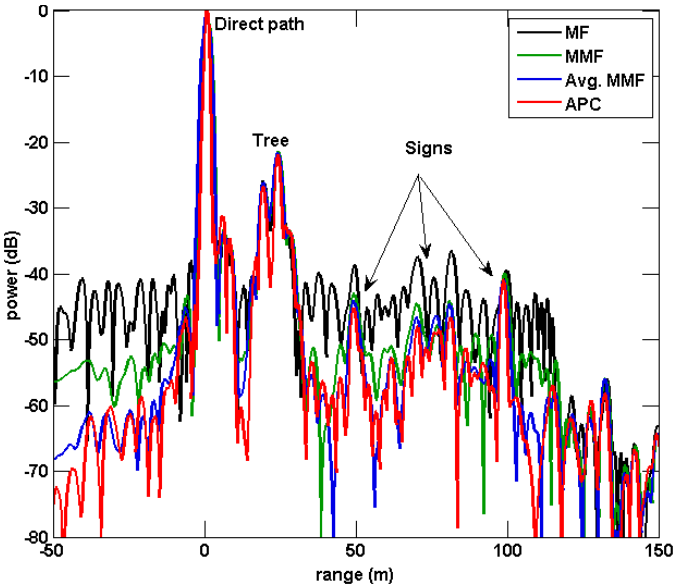

Fig. 13. Pulse compressed response using optimized FM waveform from [5] (close up)

VI. Conclusions

Optimal mismatched filtering via Least-Squares and Adaptive Pulse Compression have been devised for arbitrary FM waveforms, for which the issues of waveform/filter sampling rate, straddling effects, and possible super-resolution must be addressed. It is demonstrated using both simulated and experimentally measured results that the MMF, averaged MMF, and APC methods all surpass the sensitivity provided by the matched filter, with the averaged MMF and APC being specifically derived to provide robustness to these practical effects.

References

[1] M.A. Richards, J.A. Scheer, and W.A. Holm, *Principles of Modern Radar: Basic Principles*, SciTech Publishing, pp. 786-787, 2010.

[2] S.D. Blunt, M. Cook, J. Jakabosky, J. de Graaf, and E. Perrins, "Polyphase-coded FM (PCFM) radar waveforms, part I: implementation," *IEEE Trans. AES*, vol. 50, no. 3, pp. 2218-2229, July 2014.

[3] D.P. Scholnik, "Optimal filters for range-time sidelobe suppression," *European Signal Processing Conf.*, Tampere, Finland, 5-8 Sept. 2000.

[4] N. Levanon, E. Mozeson, *Radar Signals*, Wiley – IEEE Press, 2004.

[5] S.D. Blunt, J. Jakabosky, M. Cook, J. Stiles, S. Seguin, and E.L. Mokole, "Polyphase-coded FM (PCFM) radar waveforms, part II: optimization," *IEEE Trans. AES*, vol. 50, no. 3, pp. 2230-2241, July 2014.

[6] M.H. Ackroyd and F. Ghani, "Optimum mismatch filters for sidelobe suppression," *IEEE Trans. AES*, vol. AES-9, no. 2, pp. 214-218, Mar. 1973.

[7] J.E. Cilliers and J.C. Smit, "Pulse compression sidelobe reduction by minimization of Lp-norms," *IEEE Trans. AES*, vol. 43, no. 3, pp. 1238-1247, July 2007.

[8] A. De Maio, Y. Huang, M. Piezzo, S. Zhang, and A. Farina, "Design of radar receive filters optimized according to Lp-norm based criteria," *IEEE Trans. Signal Processing*, vol. 59, no. 8, pp. 4023-4029, Aug. 2011.

[9] S.D. Blunt, K. Gerlach, and T. Higgins, "Aspects of radar range super-resolution," *IEEE Radar Conf.*, Waltham, MA, pp. 683-687, Apr. 2007.

[10] S.D. Blunt and K. Gerlach, "Adaptive pulse compression via MMSE estimation," *IEEE Trans. AES*, vol. 42, no. 2, pp. 572-584, April 2006.

[11] S.D. Blunt, A. Shackelford, and K. Gerlach, "Single pulse imaging," *Intl. Waveform Diversity and Design Conf.*, Lihue, Hawaii, Jan. 2006.

[12] S.D. Blunt, A. Shackelford, K. Gerlach, and K.J. Smith, "Doppler compensation & single pulse imaging via adaptive pulse compression," *IEEE Trans. AES*, vol. 45, no. 2, pp. 647-659, Apr. 2009.

[13] S. D. Blunt and T. Higgins, "Dimensionality reduction techniques for efficient adaptive pulse compression," *IEEE Transactions AES*, vol. 46, no. 1, pp. 349–362, 2010.

[14] T. Yardibi, J. Li, P. Stoica, M. Xue, A.B. Baggeroer, "Source localization and sensing: a nonparametric iterative adaptive approach based on weighted least squares," *IEEE Trans. AES*, vol. 46, no. 1, pp. 425-443, Jan. 2010.

[15] T. Higgins, S.D. Blunt, and K. Gerlach, "Gain-constrained adaptive pulse compression via an MVDR framework," *IEEE Radar Conf.*, Pasadena, CA, May 2009.

[16] S.D. Blunt, K. Gerlach, and E. Mokole, "Pulse compression eclipsing repair," *IEEE Radar Conf.*, Rome, Italy, 26-30 May 2008.

[17] S.D. Blunt, T. Higgins, A. Shackelford, and K. Gerlach, "Multistatic & waveform-diverse radar pulse compression" in *Waveform Design and Diversity for Advanced Radar Systems*, eds. F. Gini, A. de Maio, and L. Patton, IET, 2012.